PERGAMON

International Journal of Heat and Mass Transfer 44 (2001) 3179–3187

International Journal of HEAT and MASS TRANSFER

www.elsevier.com/locate/ijhmt

Local heat transfer and flow distribution in a three-pass industrial heat exchanger

D.N. Sørensen [a,*], S.L. Hvid [b], M.B. Hansen [b], K.E. Meyer [a]

[a] *Department of Mechanical Engineering, Technical University of Denmark, Building 403, DK-2800 Kgs. Lyngby, Denmark*
[b] *Danish Maritime Institute, Kgs. Lyngby, Denmark*

Received 8 May 2000; received in revised form 4 September 2000

Abstract

Local heat transfer from single tubes in an industrial-sized, three-pass heat exchanger of the inline tube bundle type was measured. The transversal and longitudinal pitches were 1.8*D* and 1.5*D*, respectively, the height of each pass was 30*D* and the Reynolds number was 20 000. The measurements were made using an electrically heated cylindrical probe of the metallic film type, an instrument normally used in small-scale laboratory setups to gain detailed information about local heat transfer. The probe was positioned at various tube locations and rotated to yield the circumferential variation of the local heat transfer. Depending on location, local mean heat transfer was less than half or more than twice the nominal mean value. These variations were related to the non-uniform flow distributions present inside the heat exchanger, evidenced by computational fluid dynamics calculations. Also, the calculated velocities were used with an empirical correlation for the Nusselt number, and the results agreed very well with the measured values.

1. Introduction

Tube bundle heat exchangers are widely used in thermal and chemical process plants and their correct layout and design are crucial to the overall plant performance. One example is a three-pass, inline, cross-flow tube bundle heat exchanger considered in the present study. The heat exchanger is a half-width model of a commercial heat exchanger with six passes. Measurements were performed to investigate the influence of non-ideal flow conditions, such as the connection from the manifold to the heat exchanger and the flow between passes. It was also investigated how well a relatively simple calculation by computational fluid dynamics (CFD) could be used to predict such non-ideal flow conditions.

Among many heat transfer correlations available for design purposes, two are commonly used: Žukauskas and Ulinskas [1] and the German standard from VDI [2]. Both correlations provide an estimate of the Nusselt number based on tube pitch, fluid properties, mean velocity, and also the row number for the first few rows downstream of the inlet. Any non-uniformity of the flow, which may arise from manifolds as well as baffles in a multi-pass design, is left for the consideration of the designer. Use of computational fluid dynamics, e.g. by representing the tubes as local resistances, enables the overall flow distribution to be predicted, thus aiding the design.

A large number of experimental investigations are described in the literature. The electrically heated metallic film technique, described in, e.g. Baughn et al. [3], is used for some of these studies. In Baughn et al. [4], this method is used to measure the local heat transfer of a single cylinder, two cylinders in tandem, and a cylinder at the entrance region of a tube bundle. Also, many of the measurements in [1,5] are carried out using an electrically heated metallic film. Using laser Doppler anemometry (LDA), Meyer [6] found several asymmetric flow patterns in a small tube bundle with seven rows, each consisting of three tubes and two semi-tubes at the side walls. Extending the investigation, Meyer [7] used the heated gold-film technique to

* Corresponding author. Tel.: +45-4525-4300; fax: +45-4593-0663.
E-mail address: dns@mek.dtu.dk (D.N. Sørensen).

0017-9310/01/$ - see front matter
PII: S0017-9310(00)00356-2

Nomenclature

D	tube diameter
h	local heat transfer coefficient
$\overline{h}$	average heat transfer coefficient
L	distance between electrodes on measuring probe
Nu	local (circumferential) Nusselt number
$\overline{Nu}$	average Nusselt number from measurements, Eq. (2)
$\overline{Nu}_Z$	average Nusselt number from correlation, Eq. (3)
Pr_f	Prandtl number at fluid temperature
Pr_w	Prandtl number at cylinder wall temperature
q''_{cond}	conduction from the gold coating into the probe
q''_{conv}	convective heat flux from the probe to the surrounding air
q''_{el}	electrically produced heat flux
q''_{rad}	radiation from the probe surface to the surroundings
R''	local surface resistance (resistance of square section of coating)
R''_β	local surface resistance at T_β
Re	Reynolds number, $Re = U_m D/v$
S_1	transversal pitch
S_2	longitudinal pitch
T	temperature
ΔT	difference between fluid temperature and local gold film temperature
ΔT_{wall}	temperature difference between fluid and probe wall
T_β	reference temperature for the surface resistance calibration
U_m	velocity in minimum cross-section
V_{el}	voltage across the measuring probe

Greek symbols

β	temperature coefficient of resistance at T_β
ϵ_{gold}	emissivity of the plastic film
λ	thermal conductivity
v	kinematic viscosity

measure the local heat transfer for the asymmetric flow fields. The tube arrangement in [6,7] is the same as in the present study.

It is the purpose of the present study to measure the local heat transfer at different locations in a full-scale heat exchanger, and to relate the observed variations to computed flow fields. To the authors' knowledge, all of the previously mentioned investigations, in which the electrically heated metallic film technique has been used, have been carried out in small-scale laboratory facilities with ideal setups, i.e. uniform inlet velocity and carefully positioned tubes, whereas the present work applied the method to an industrial-sized heat exchanger, where the measurement probe, in turn, replaced tube sections within the heat exchanger. Selection of the measurement positions was based mainly on the CFD calculations of the flow field, where the tube rows were modelled by volume forces, but also on measurements with LDA and pitot-tubes.

Data, represented by circumferential distributions of local Nusselt numbers, are presented for: an inlet with a recirculating zone in the plane of the tubes; a turn with a recirculating zone along the tubes; and a position where the flow was fully developed. Furthermore, the distributions were integrated to provide the average Nusselt number and, locally, in inlet regions as well as after turns, the Nusselt number varied from less than half to more than twice the value obtained for a tube position where the flow was fully developed. To extract quantitative information from the CFD calculations, the design correlation of Žukauskas and Ulinskas [1] was used with the local velocities determined from the CFD calculations and, except in recirculating zones, the agreement was found to be very good, implying that a relatively simple CFD model may be used to gain important information about the local properties within a complex heat exchanger.

2. Methods

2.1. The heat exchanger

Fig. 1 shows a side view of the heat exchanger setup. The heat exchanger module was connected to a manifold, which in industrial applications would feed several identical modules. When leaving the manifold, the flow turned 90° to enter the first pass of the heat exchanger. It was then reversed into the second pass and, after passing the tubes again, a second flow reversal led the flow into the third pass and the exit. Each of the three passes involved 36 rows with 10 tubes in each row. The tubes were smooth with an outer diameter (D) of 40 mm. The transversal and longitudinal pitches of the tubes were $S_1 = 1.8D$ and $S_2 = 1.5D$, respectively. The height of the first pass of the heat exchanger was approximately $30D$, whereas the height of the second and third passes was around $28D$. The distance between the walls of the heat exchanger and the perimeter of the outermost tubes was $0.8D$. In the description of tube positions, the front and back of the heat exchanger in Fig. 1 are denoted as A-side and B-side, respectively.

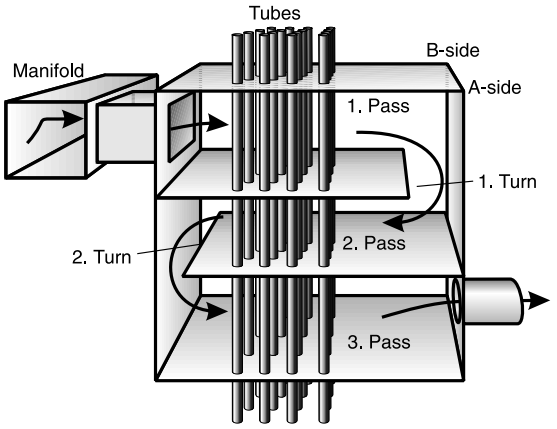

Fig. 1. Side-view sketch of the heat exchanger showing the inlet turning the flow from the manifold into the heat exchanger, the expansion before the tube bundle, the two turns, and finally the outlet.

2.2. Flow setup

To simulate a situation in which several modules of the heat exchanger were connected to one manifold, only one third of the flow through the manifold entered the heat exchanger (Fig. 1). The rest of the flow left through an adjustable grid at the end of the manifold, simulating the pressure loss from other heat exchanger modules. To lower the forces on the walls of the heat exchanger, the pressure inside the heat exchanger was kept near atmospheric pressure by using two radial blowers to drive the flow: one upstream of the manifold and one immediately downstream of the heat exchanger module. The flow rate through, and pressure inside the heat exchanger were adjusted by regulating the two blowers as well as the blockage of the grid at the outlet from the manifold.

The flow rate through the heat exchanger was measured after the second blower, using an orifice plate, in accordance with the ISO 5167 standard [8]. The fluid temperature inside the heat exchanger was around 300 K. To enable optical access for the LDA system, the A-side and the two end walls of the heat exchanger were constructed using 10 mm thick glass plates. The B-side was covered with 2 mm steel plates.

2.3. Heat transfer measuring technique

The experimental technique used to measure the local heat transfer was almost the same as reported in [3] and later in [7]. A plastic film with a thin gold coating was used to produce an electrical heating with an almost uniform heat flux. From measurements of the difference between the local wall temperature and the free stream temperature, the local heat transfer coefficient was determined.

The film was made of 0.17 mm thick transparent thermoplastic polyester (Courtaulds Performance Films, USA) with a gold coating giving a nominal surface resistance of $R'' = 2\ \Omega$. Seven thermocouples were glued to the back of the film: five thermocouples were equally spaced along a tube perimeter, centered between the ends of the probe, and two thermocouples were located at a distance of one diameter up and down, respectively, from the other thermocouples (Fig. 2). The test tube, measuring $6D$ in length, was made by bracing the coated film against the inner wall of a cylindrical mould. Plastic fittings were fixed to each end of the film, and the cylindrical mould filled with a self-expanding foam creating an insulating support for the film.

Electrodes made of copper foil were glued onto the ends of the plastic foil with a silver-loaded epoxy glue. The electrodes were attached to a power supply and a voltmeter by a four-wire connection. Furthermore, the thermocouples were connected to the voltmeter (a Hewlett-Packard HP34970A data acquisition/switch unit) and to a cold junction located in the free air stream. Hence, the voltage from a thermocouple gave the desired temperature difference. The voltmeter had a resolution of 0.1 μV, corresponding to 0.0025 K. The thermocouples were mounted in the cylinder and calibrated using the voltmeter described above. The accuracy of the measurement of the temperature difference was estimated to be ±0.1 K.

2.4. Data reduction

One notable difference between the configuration used by Meyer [7] and the present configuration was that the plastic film in the present configuration had the gold-coated side turned towards the insulating support and not towards the surroundings. This gave a more robust instrument, but also introduced two extra sources of uncertainty: an additional temperature difference due to

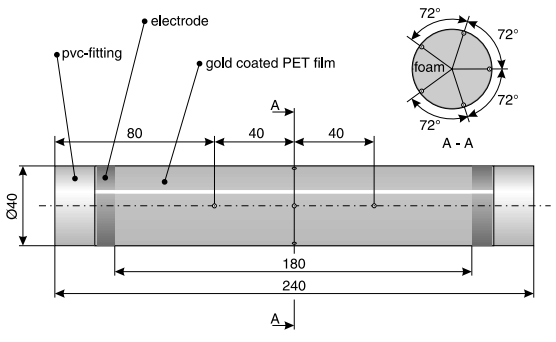

Fig. 2. Measuring tube. Positions of thermocouples are indicated with ⊙.

heat conduction through the plastic film and, furthermore, significantly higher radiation to the surroundings because the emissivity of the plastic film is higher than the emissivity of the gold coating.

Although the measuring tube was designed to give a constant heat flux from the surface, small variations occurred and a correction was introduced in order to obtain, accurately, the local Nusselt numbers. The heat flux q''_{el} produced by the electrical heating of the gold coating was absorbed by three processes: convection q''_{conv} to the air; conduction q''_{cond} from the gold coating into the probe; and radiation q''_{rad} from the surface to the surroundings (assuming uniform temperature of the surroundings). The emissivity of the plastic film was $\epsilon_{gold} = 0.83$ [9]. The internal conduction q''_{cond} was found from a finite difference analysis of the measuring tube, using the measured temperature at the gold coating as boundary condition. The temperature difference between the fluid and probe wall, ΔT_{wall}, was found by taking the measured temperature difference between fluid and gold coating, ΔT, and subtracting the temperature difference over the plastic film. The temperature difference over the plastic film was determined from the local heat flux through the film: $q''_{el} - q''_{cond}$. The radiation q''_{rad} was found using the wall temperature and the measured fluid temperature. Finally, the convection to the air was found as $q''_{conv} = q''_{el} - q''_{cond} - q''_{rad}$, and the local heat transfer coefficient as $h = q''_{conv}/\Delta T_{wall}$.

The electrical resistance of the gold coating was not completely uniform and two effects were taken into account: the temperature dependency and non-uniformities in the gold coating. Assuming that the local surface resistance could be described as $R'' = R''_{\beta}(1 + \beta(T - T_{\beta}))$, where β is the temperature coefficient of resistance and R''_{β} the local surface resistance at T_{β}, and where both R''_{β} and β were found by calibration [7]; the electrically produced local heat flux could be described by

$$q''_{el} = \frac{(V_{el}/L)^2}{R''_{\beta}(1 + \beta(T - T_{\beta}))}, \tag{1}$$

where V_{el} is the voltage applied over the electrodes and L is the distance between the electrodes. The voltage was adjusted to provide a ΔT between 3 and 9 K which was judged to give reasonable accuracy without overheating the probe.

The local Nusselt number was found as $Nu = hD/\lambda$, where λ is the thermal conductivity. The measured wall temperature represented an adiabatic wall temperature and therefore depended on the flow velocity. The adiabatic heating was found to be less than 0.1 K and no conversion to static temperature was applied. The average heat transfer coefficient, $\overline{h}$, was defined as the ratio between the average heat flux and the average temperature difference between the surface temperature and the upstream temperature. From the average heat transfer coefficient, the average Nusselt number was calculated as

$$\overline{Nu} = \frac{\overline{h}D}{\lambda}. \tag{2}$$

The thermal conductivity λ and the kinematic viscosity v were both evaluated at the free stream temperature. The total uncertainty of the measured Nusselt numbers was estimated to be $\pm 5\%$.

2.5. Flow simulations

Before carrying out any measurements, the commercial CFD program STAR-CD [10] was used to obtain an estimate of the flow field in the heat exchanger. This way, areas with particularly interesting flow phenomena were identified for later measurements with LDA or with the gold-film probe.

The isothermal, steady Reynolds-averaged Navier–Stokes equations were solved with a standard high Reynolds number k–ϵ model employing the normally quoted coefficients [11]. The flow field was solved isothermally, thus corresponding to the experimental investigations. The influence from each row of tubes was modelled using volume forces, evenly distributed across the width of the heat exchanger. Based on the preliminary numerical investigations, the distributed resistance was represented by porous baffles rather than porous cells because the latter appeared to dampen the flow in the transverse directions too strongly. The user-defined coefficients in the expression for the velocity-dependent pressure loss across the baffle were determined from correlations of the pressure loss across similar tube bundles [12].

A first-order upwinding difference scheme was used for the convective terms. An investigation was carried out in two dimensions, comparing the first-order scheme with second- and third-order schemes, and it was found that the first-order upwinding scheme was sufficiently accurate for the present purpose. To limit memory requirements, the computational problem was divided into two parts. (1) an inlet part, covering the manifold and the first pass, using approximately 340.000 computational cells and (2) a part covering the flow passage from the second to the third pass (290.000 cells). The entry flows to the second and third pass were assumed to be similar. The geometrical size of the computational cells was $0.75D$. Thus, each row of tubes was described by two cells in the streamwise direction.

2.6. Heat transfer correlation

The measured average Nusselt numbers, obtained by Eq. (2), were compared with the following correlation for the average Nusselt number in inline tube bundles [1]:

$$\overline{Nu}_Z = 0.27 Re^{0.63} Pr_f^{0.36} (Pr_f/Pr_w)^{0.25}, \tag{3}$$

which applies for Reynolds numbers, $Re = U_m D/v$, ranging from 10^3 to 2×10^5, where U_m is the mean velocity in the minimum cross-section between the tubes. Since large variations in velocity appeared locally in the setup, it was not possible to define a local Reynolds number from the measurements. However, calculating an average value of U_m as the flow rate divided by the minimum cross-sectional area, the Reynolds number was around 17 300 in the first pass of the heat exchanger and around 19 000 in the second and third passes. Due to the limited temperature difference between tube wall and fluid the Prandtl number was assumed constant, $Pr_f = Pr_w = 0.708$.

To enable a comparison between the measured value of the Nusselt number (Eq. (2)), and the correlation value (Eq. (3)), the predicted velocities from the CFD calculations were extracted at the measurement positions, and the local velocity was calculated from the velocity components perpendicular to the tube axis, thus neglecting the flow in the tubewise direction. Implicitly, the validity of Eq. (3) requires that the distance between the side walls and the tube bundle should be half the transversal inter-tube distance which, in the present case would result in a gap of $0.4D$, rather than the actual gap of $0.8D$. Preliminary experimental investigations (not shown) of the Nusselt number for gaps of $0.4D$, $0.65D$, and $0.8D$ indicated that, apart from the outer tubes of the bundle, the correlation in Eq. (3) could correctly predict the variation in Nusselt number as a function of the gap size, if the gap was included in the calculation of cross-sectional areas. In the CFD calculations, the volume forces, modelling each row of tubes, were applied across the whole width of the heat exchanger and did not consider the gap size. To determine the velocity in the minimum cross-section, U_m, the velocity from the CFD calculations was multiplied by the ratio between the maximum cross-sectional area and the minimum cross-sectional area, both calculated with the excessive $0.8D$ gap size.

Žukauskas and Ulinskas [1] describes a correction to Eq. (3) for the first tubes in the bundle to account for the lowered turbulence intensity in this region. The first tubes of the heat exchanger considered here were either positioned after the 90° turn into the heat exchanger, or after the baffles, reverting the flow into the following pass. Thus, it was believed that the turbulence intensity was high from the very beginning of the bundle, and the correction was not applied.

3. Results

First, the velocity distribution at various positions in the heat exchanger, estimated by the CFD calculations, is shown. Following this, the measurement program and representative results for the heat transfer, found using the gold-film probe, are presented.

3.1. CFD Calculations

In Fig. 3, the predicted flow in the first pass is depicted in a horizontal plane, positioned halfway between the top and bottom. The 90° bend from the manifold into the heat exchanger results in a large recirculating zone and significantly influences the flow in the first 14 rows. In particular, a very large velocity is observed at the B-side and a very small velocity is observed at the A-side. Furthermore, the direction of the flow is from the B-side towards the A-side for the first 10 rows, after which a slight flow from the A-side towards the B-side appears. After approximately 20 rows, the horizontal velocity variations are gone.

Fig. 4 shows the predicted velocity distribution in the position between the second and the third passes. The plane of view is centered between the sides of the heat exchanger. Due to the 180° turning of the flow, a recirculating zone appears in the upper part of the third pass, influencing the flow for the first 10 tube rows. Most significantly, in the first few rows, the velocity in the lower part of the pass is very large, compared to the velocity in the upper part of the pass, where the recirculating zone is found.

3.2. Heat transfer measurements

By rotation of the probe, the measurements were performed with a circumferential resolution of 6°. Only a limited number of measurements could be performed with the gold-film probe, and much consideration was

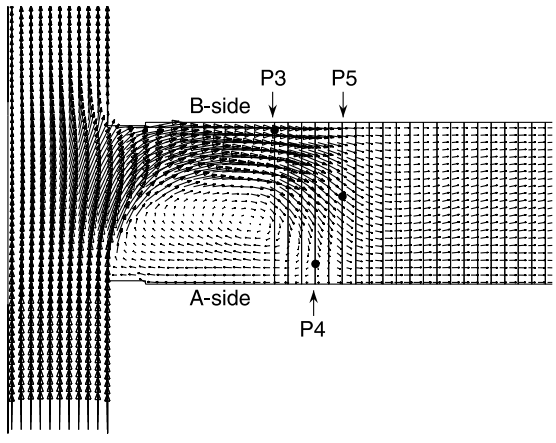

Fig. 3. 1 Pass, top view, vertically centered: calculated velocity distribution. Each line between the two walls signifies a row of tubes. Circles mark the measurement positions.

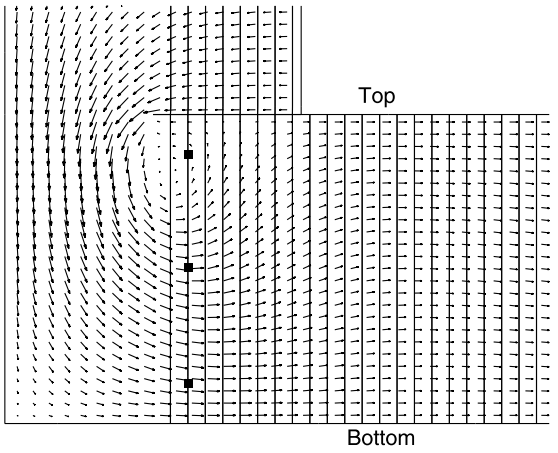

Fig. 4. Flow between passes, side view, centered between the walls: calculated velocity distribution. Each line signifies a row of tubes. Squares mark the measurement positions, $P2$.

given to the selection of measurement positions. It was assumed that the flow field, predicted by the CFD calculations, was in reasonable agreement with the conditions actually present in the experimental heat exchanger.

A position in row 30, five tubes from the B-side were selected for the measurement of fully developed flow, since the velocity variations described by the CFD calculation (Fig. 4) disappeared after approximately 10 rows. The measuring probe was vertically centered. Denoting this tube position as P_1, Fig. 5 shows the

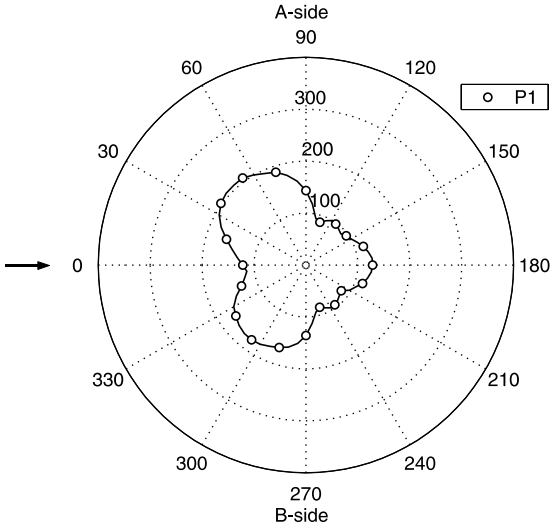

Fig. 5. Measured distribution of the Nusselt number in the second pass, row number 30, five tubes from the B-side (position P_1). The arrow shows the throughflow direction, and every third measurement point is marked with a symbol.

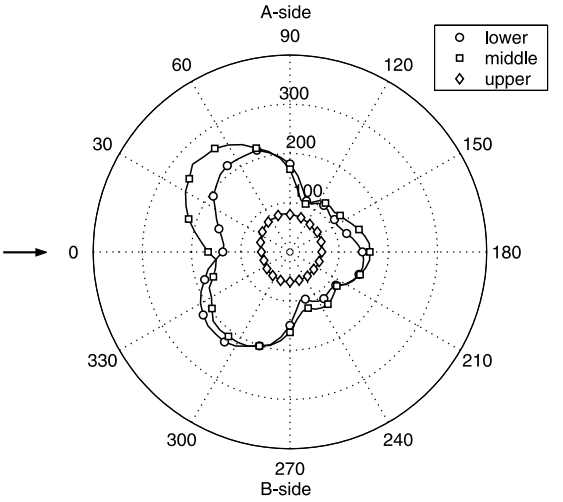

Fig. 6. Measured distributions of the Nusselt number at the inlet to the second pass, 2. row, five tubes from the B-side (position P_2). The arrow shows the throughflow direction, and every third measurement point is marked with a symbol.

circumferential distribution of the Nusselt number presented as a polar plot.

The recirculating zone at the inlet of the second pass (see the CFD calculation of Fig. 4) was investigated by measuring in three vertical positions at the second row of the second pass, five tubes from the B-side (position P_2). The measured distributions of the Nusselt number for the three positions are shown in Fig. 6.

To examine the inlet conditions of the heat exchanger, three positions were chosen based on the CFD calculation (Fig. 3): a high velocity position (first row, at the B-side, denoted P_3); a low velocity position (fourth row, second tube from the A-side, denoted P_4); and at a position with skewed flow direction (sixth row, fifth tube from the B-side, denoted P_5). In Fig. 7, the measured distributions of the Nusselt number are depicted.

Using Eq. (2), the integrated values of the Nusselt number ($\overline{Nu}$) were calculated for the above-measured distributions (Table 1). The table also contains the Reynolds number based on U_m, calculated as the measured flow rate divided by the minimum cross-section. The small differences in Re were caused by variations in temperature, flow rate, etc. during the measurement period. The difference in Re between the first and the second pass was mainly due to the different heights of the two passes. Using the design correlation, Eq. (3), with the local velocities from the CFD calculations, the predicted value, $\overline{Nu}_Z$ was calculated, and the relative difference between the measured and the predicted Nusselt number is included in Table 1.

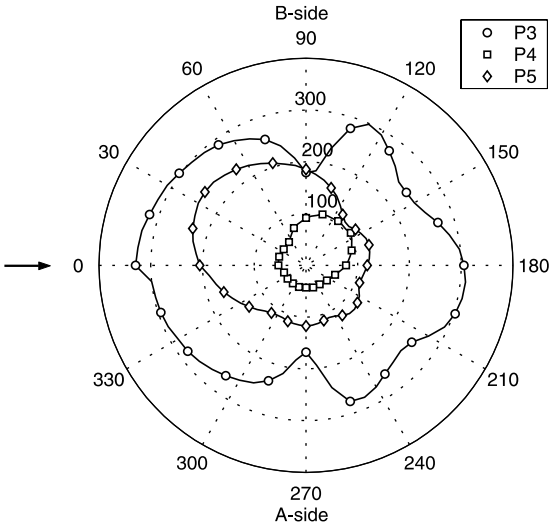

Fig. 7. Measured distributions of the Nusselt number in the inlet section of the heat exchanger. Position P_3 is at the B-side, first row, P_4 is the second tube from the A-side in the fourth row and P_5 is the fifth tube from the B-side in the sixth row. The arrow shows the throughflow direction, and every third measurement point is marked with a symbol.

Table 1
Reynolds number, measured Nusselt number and relative difference between measured and predicted Nusselt number[a]

Tube position	Re	$\overline{Nu}$	$(\overline{Nu}-\overline{Nu}_Z)/\overline{Nu}_Z$ [%]
P_1	19 100	126	6
P_2, lower	19 000	148	−4
P_2, middle	18 900	160	7
P_2, upper	19 100	64.3	73
P_3	17 300	262	−3
P_4	17 300	58.5	−7
P_5	17 300	142	15

[a] The predictions were based on the CFD calculations.

4. Discussion

An important issue when designing a heat exchanger is to create a velocity distribution close to uniform across the heat exchanger, ensuring that all tubes in the heat exchanger have the same performance. Further, the pressure loss across the tube is proportional to the velocity squared which, when integrated across the heat exchanger, yields the least value for a uniform velocity distribution. Finally, from Eq. (3) it is seen that the heat transfer is proportional to the velocity to a power of 0.63. Non-uniformities in the velocity distribution are thus likely to reduce the total heat transfer of the heat exchanger. In the following, some of the characteristics of the local Nusselt number distribution of the five different measurement positions are discussed.

Position P_1: This tube was positioned in a downstream row, centered between the walls and thus expected to be representative of the majority of tubes in the bundle. The circumferential distribution of the Nusselt number is shown in Fig. 5. For inline tube bundles, the circumferential Nusselt number distribution is characterized by [1]: (1) a minimum value at the frontal point, which is inside the recirculating zone of the upstream tube, (2) a maximum some distance from the frontal point where the flow from the upstream tube collides with the tube wall, followed by a decrease, (3) an increase because of laminar/turbulent transition, followed by a decrease and (4) an increase due to separation of the turbulent boundary layer. All of the above properties can be seen in Fig. 5, confirming the accuracy and resolution of the gold-probe measurements.

The distribution was slightly asymmetrical, which was probably due to small imperfections in the construction of the heat exchanger. However, this does not influence the above discussions. The measurements were made at several positions along the tube, all with similar distributions, and the large asymmetries observed in the small tube bundle in [6,7] were not found in the present experiment.

Position P_2: This position was in the second row, following the 180° turn into the second pass (Fig. 4). Three vertical positions were investigated for this tube (Fig. 6), and the upper position had significantly lower values of local Nusselt number than the middle and the lower positions. Furthermore, the shape of the upper distribution was different, almost circular, which strongly indicates that no preference existed for the flow direction, thus supporting the presence of the recirculating zone in the inlet to the second pass, predicted by the CFD calculations (Fig. 4). On the contrary, the shape of the distributions for the two other vertical positions resembled the one found for position P_1 (Fig. 5).

Position P_3: At the inlet to the first pass of the heat exchanger, a large recirculating zone was predicted by the CFD calculation (Fig. 3). The heat transfer in position P_3 was expected to be very large since the velocity was large, and this was confirmed by the circumferential measurements of the heat transfer in Fig. 7. Because position P_3 is in the very first row of tubes, the circumferential distribution of the Nusselt number should, qualitatively, resemble the distribution for a single tube. According to [1], the Nusselt number distribution for a single tube has a maximum in the frontal point after which a decrease occurs until around 90°. After this, the Nusselt number increases until the rear point of the tube. From Fig. 7, the resemblance is reasonable since a maximum in Nusselt number occurred at the frontal point and a minimum around 90°. However, from 115° to 150°, a second decreasing region was observed which does not appear for the single tube. This

discrepancy compared to the single tube is probably because of the influence from the other tubes in the row which may alter the circumferential distribution of the Nusselt number, especially at the rear part of the tube [1].

Position P_4: According to the CFD calculation, this position was in the low-velocity region of the recirculating area (Fig. 3). This agreed with the circumferential distribution of the Nusselt number, marked with squares in Fig. 7, which was very low and symmetrical around 130°, indicating that the flow direction was towards the inlet of the heat exchanger. Thus, the measurements confirmed the recirculating zone predicted by the CFD calculation.

Position P_5: Finally, position P_5 was in the sixth row in the inlet of the heat exchanger. According to the CFD calculation (Fig. 3), this was after the recirculating zone but before the flow was fully developed. The circumferential distribution of Nusselt number was symmetrical around 36°. For the CFD calculation the flow angle at the same position was 38° and thus a very good agreement existed at this point. Furthermore, the measured distribution of the Nusselt number did not resemble a typical inline tube (as discussed in relation to position P_1). Especially in the symmetry point, a maximum of the Nusselt number occurred, which resembled the appearance of a single tube or a tube in a staggered tube bundle [1]. This was probably due to the 36° flow angle actually enabling the flow to pass between the tubes of the previous row, which thus resembled a staggered tube bundle.

Integrated values: Table 1 contains the measured, integrated Nusselt numbers, in the column labelled $\overline{Nu}$. Inside recirculating zones (P_2, upper and P_4) the Nusselt numbers were around 60, thus only half of the representative value of $\overline{Nu} = 126$ in position P_1. For the high-velocity position, at the inlet to the first pass, P_3, the Nusselt number was 262, and thus more than twice the representative value of position P_1. At positions P_2, middle and lower, following the turn, the Nusselt number was higher than at P_1 because of the increased velocity outside the recirculating zone, necessary for mass conservation. Finally, at position P_5, the Nusselt number was higher than at P_1 because the tube arrangement made the bundle appear staggered rather than inline for the local flow direction, thereby increasing the Nusselt number. To summarize, very large variations existed throughout the heat exchanger, all of which could be explained by the large variations in velocity, evidenced by the CFD calculations.

To obtain quantitative information from the CFD calculations, the last column in Table 1 contains the relative difference between the measured value of the Nusselt number and the correlated value based on the local velocities from the CFD calculations. The seven measurement positions may be divided into three groups:

1. *Streamwise flow*: For positions P_1, P_2, lower, P_2, middle, and position P_3, the flow was in the expected direction along the inline bundle. Therefore, the correlation in Eq. (3) was expected to be valid if the correct local velocity was used for the evaluation of the Reynolds number. As seen from Table 1, the relative difference between correlation and measurements for these positions were all within 7%, even though the actual values of the Nusselt numbers varied between 126 and 262. Thus, for flows with inline direction, the velocities determined from the CFD calculation could be used successfully in the design correlation to yield the Nusselt numbers, locally inside the heat exchanger.
2. *Recirculating flow*: For positions P_2, upper and P_4, the measurements were inside large recirculating zones, and the correlation was not expected to give reasonable results because the flow inside a recirculating zone is not along the inline direction and the correlation therefore invalid. Also, the CFD calculation was steady and thus could result in very small velocities, whereas, in the actual setup, the flow is inherently unsteady. From Table 1, the relative difference between correlation and measurements were 73% for P_2, upper, and 7% for P_4 and from the above, the close agreement for P_4 must be a coincidence.
3. *Skewed flow*: For position P_5, the flow was skewed 36° from the streamwise direction, and the measurement was 15% above the correlation, even though the velocity from the CFD calculation included the transversal velocity component. The circumferential distribution of the Nusselt number in this position resembled a tube inside a staggered bundle because of the skewed flow. Generally, staggered tube bundles have higher Nusselt numbers than inline bundles [1], and this is probably the reason for the excessive value of the measured Nusselt number in position P_5.

5. Conclusions

The heated gold-film technique was used to measure the variations in heat transfer in a three-pass industrial heat exchanger of the inline tube bundle type. The method provided accurate information concerning the circumferential heat transfer characteristics. Besides providing the integrated Nusselt number, the circumferential distributions gave information about the flow past individual tubes, and the influence from upstream tubes and recirculating zones in the heat exchanger could be determined.

For the heat exchanger considered in the present study, the influence from recirculating areas in the inlet as well as after the turns was large, and Nusselt numbers varied from half the nominal mean value in some parts

of the heat exchanger to twice the nominal mean value in other parts.

Furthermore, CFD was used as a tool to identify regions of special interest which were investigated using the gold-film probe. Comparing the CFD calculations with the local Nusselt number distributions showed that the CFD calculations were able to capture the main characteristics of the flow field. Furthermore, local velocities from the CFD calculations were used as input to the design correlation from [1], resulting in very good predictions of the average Nusselt numbers, except inside recirculating zones. Throughout the study, a very good agreement between the calculated flow field and the measured heat transfer was found. Thus, this study implies that a relatively simple CFD calculation can be used to gain information about the heat transfer in a complex geometry heat exchanger.

Acknowledgements

The study was partially supported by the Danish Research Council under grant STVF 9502261 and the Danish Agency for Trade and Industry. Furthermore, the authors appreciate the discussions with Prof. P.S. Larsen.

References

[1] A. Žukauskas, R. Ulinskas, Heat Transfer of Tube Banks in Crossflow, Experimental and Applied Heat Transfer Guide Books, Hemisphere, Washington, DC, 1988.

[2] VDI. VDI-Wärmeatlas. Berechnungsblätter für den wärmeübergang. Siebte, erweiterte Auflage. VDI-Verlag, 1994.

[3] J.W. Baughn, R.K. Takahashi, M.A. Hoffman, A.A. McKillop, Local heat transfer measurements using an electrically heated thin gold-coated plastic sheet, J. Heat Transfer, Trans. ASME 107 (1985) 953–959.

[4] J.W. Baughn, M.J. Elderkin, A.A. McKillop, Heat transfer from a single cylinder, cylinders in tandem, and cylinders in the entrance region of a tube bank with a uniform heat flux, J. Heat Transfer, Trans. ASME 108 (1986) 386–391.

[5] A. Žukauskas, J. Žiugžda, Heat Transfer of a Cylinder in Crossflow, Experimental and Applied Heat Transfer Guide Books, Hemisphere, Washington, DC, 1985.

[6] K.E. Meyer, Three-dimensional effects of turbulent flow in an in-line tube bundle, in: Proceedings of the Ninth International Symposium on Applications of Laser Techniques to Fluid Mechanics, Lisbon, Portugal, 1998, pp. 20.1.1–20.1.8.

[7] K.E. Meyer, Local heat transfer from a tube bundle in an in-line tube bundle with asymmetrical flow, in: B.J. Grochal, J. Mikielewicz, B. Sundén (Eds.), Progress in Engineering Heat Transfer, Institute of Fluid-Flow Machinery Publishers, Gdańsk, Poland, 1999, pp. 399–406.

[8] ISO. Measurements of fluid flow by means of pressure differential devices. International Standard 5167-1:1991(E), ISO, 1991.

[9] M.H. Hansen, Heat transfer in tube bundles. Master thesis ET-EP 98-08, Department of Energy Engineering, Technical University of Denmark, DK-2800 Kgs. Lyngby, March 1998.

[10] STAR-CD. Manual version 2.3. Computational Dynamics Limited, 1995.

[11] B.E. Launder, D.B. Spalding, The numerical computation of turbulent flow, Comput. Meth. Appl. Mech. Eng. 3 (2) (1974) 269–289.

[12] I.E. Idelchik, Handbook of Hydraulic Resistance, CRC Press, Boca Raton, 1994.